

# Accounting for Model Errors in Ensemble Data Assimilation

Hong Li

*Laboratory of Typhoon Forecast Technique, Shanghai Typhoon Institute of CMA,*

*Shanghai, China*

Eugenia Kalnay and Takemasa Miyoshi

*Department of Atmospheric and Oceanic Science, University of Maryland, College*

*Park, MD*

Christopher M. Danforth

*Department of Mathematics & Statistics, Complex Systems Center, Vermont Advanced*

*Computing Center, University of Vermont, Burlington, VT*

Submitted to *Monthly Weather Review* for publication

(Revised: January 6, 2009)

---

*Corresponding author address:* Hong Li, Shanghai Typhoon Institute, 166 Puxi Road,  
Shanghai, China, 200030. E-mail: [lih@mail.typhoon.gov.cn](mailto:lih@mail.typhoon.gov.cn)

## **Abstract**

This study addresses the issue of model errors with the ensemble Kalman filter. Observations generated from the NCEP/NCAR reanalysis fields are assimilated into the SPEEDY model. Absent an effort to account for model errors, the performance of the Local Ensemble Transform Kalman Filter (LETKF) is seriously degraded when compared to the perfect model scenario. Several methods to account for model errors, including model bias and system-noise, are investigated. The results suggest that the two pure bias removal methods considered (DdSM and LDM) are not able to beat the multiplicative or additive inflation schemes used to account for the effects of total model errors. In contrast, when the bias removal methods are augmented by additive noise representing random errors (DdSM+ and LDM+), they outperform the pure inflation schemes. Of these augmented methods, the LDM+, where the constant bias, diurnal bias and state-dependent errors are estimated from a large sample of 6-hour forecast errors, gives the best results. The advantage of the LDM+ over other methods is bigger in data sparse regions than in data dense regions.

## 1. Introduction

After more than 10 years of research, variants of the Ensemble Kalman Filter (EnKF) proposed by Evensen (1994) are now becoming viable candidates for the next generation of data assimilation in operational NWP. The advance is primarily due to the fact that (1) they include a flow-dependent background error covariance; 2) they are easy to code and implement; and 3) they automatically generate an optimal ensemble of analysis states to initialize ensemble forecasts. Many studies to date have tested EnKF systems under the perfect model assumption with simulated observations, and only within the last few years have EnKF assimilating real atmospheric observations been tested (e.g., Houtekamer et al. 2005; Whitaker et al. 2008; Szunyogh et al. 2008; Torn and Hakim 2008; Meng and Zhang 2008). Notably, an EnKF has been operational since 2005 in the Canadian Meteorological Centre (Houtekamer and Mitchell 2005) and when using the same model and observations, the EnKF scores are about the same as the 4D-Var scores<sup>1</sup>.

In practice, forecast errors derive not only from errors in the initial conditions but also from errors due to model deficiencies. The latter type of error is usually called *model error*. Model error can be due to lack of resolution, approximate parameterizations of physical processes, numerical discretization, etc. For assimilation of real observations, assuming that the model is perfect is overly optimistic (Dee 1995). In this case, the ‘true’ forecast error covariance should include uncertainties from both inaccurate initial condition and model errors. As a result, the

---

<sup>1</sup> [http://4dvarenkf.cima.fcen.uba.ar/Download/Session\\_7/Intercomparison\\_4D-Var\\_EnKF\\_Buehner.pdf](http://4dvarenkf.cima.fcen.uba.ar/Download/Session_7/Intercomparison_4D-Var_EnKF_Buehner.pdf)

background error covariance in EnKF associated with errors associated only with the initial conditions is smaller than the ‘true’ forecast error covariance because it does not account for the second type of forecast error. To address this problem, most applications account for model errors by simply enlarging the background error variance (multiplicative inflation, Anderson and Anderson 1999), adding additional terms to the background error variance (additive inflation, Mitchell and Houtekamer 2000; Mitchell et al. 2002; Hamill and Whitaker 2005; Corazza et al. 2007; Whitaker et al. 2008). Though these techniques are easy to implement, they account for model error within the second moment of the ensemble by enlarging the background ensemble spread, rather than directly correcting the model errors in the ensemble mean. Another approach has been to use different physical parameterization schemes (Fujita et al. 2007; Meng and Zhang 2007, 2008). Dee and da Silva (1998) proposed a method for the on-line estimation and correction of model bias from the ensemble mean. This bias correction method (DdSM, hereafter) has been successfully tested, for example, by Dee and Todling (2000), Carton et al. (2000), Chepurin et al. (2005), Keppenne et al. (2005). Recently, Baek et al. (2006) developed another bias correction method similar to the DdSM except that it allows for “adjusting” the observations, rather than the model bias, and it accounts for the cross-correlation of uncertainties in model state and bias that had been ignored in the DdSM. They successfully tested this approach with the Lorenz-96 model. However, both of these two methods assume that the bias is static in time, resulting in estimates of only the slowest varying component of model error. In reality, model error likely varies with time (e.g., errors in the

diurnal cycle) or with the state of the atmosphere (e.g., biases are different during an El Niño episode).

Danforth et al. (2007) proposed an approach where the state-independent model error (bias) was estimated from the average of a large ensemble of 6-hour forecast minus analysis fields (i.e., 6-hour apparent forecast errors), diurnal errors were estimated from the dominant Empirical Orthogonal Functions (EOFs), and state-dependent errors were determined using the leading terms in a Singular Value Decomposition. They found this low-dimensional method (LDM, hereafter), where the state-dependent errors are expressed in terms of very few degrees of freedom (d.o.f.), to be very successful and computationally efficient. This method has been successfully tested with the coupled Lorenz-96 model (Danforth and Kalnay 2008) and the simple but realistic global SPEEDY model (Danforth et al. 2007). However, in both studies there is no data assimilation involved since the initial conditions were taken to be a system trajectory and the NCEP-NCAR Reanalysis, respectively. It is worthwhile to expand the application of the LDM to more realistic situations where the forecast-analysis is cycled and, as a result, forecast error includes both model error and dynamical growing error due to the imperfect initial condition.

In this study we investigate the performance of an ensemble Kalman filter in a perfect model and in the presence of significant model errors and then apply different approaches to deal with model errors in ensemble data assimilation. The Local Ensemble Transform Kalman Filter (LETKF, Hunt et al. 2007) is used as a representative of other EnKF systems. A review of the LETKF is given in section 2.

The different techniques for treating model errors are described in section 3. Section 4 contains the performance of the LETKF in a perfect model scenario. In section 5, the LETKF performance in the presence of model errors due to assimilating observations generated from the NCEP/NCAR reanalysis fields is examined. Two inflation schemes (multiplicative and additive inflation) and two bias correction methods (DdSM and LDM) are applied to account for and/or correct model errors. Their results are compared and discussed in both a uniform and a rawinsonde-like observation network. Section 6 gives our summary and discussion.

## 2. LETKF data assimilation scheme

The LETKF is one of the ensemble square-root filters (Tippett et al. 2003) in which the observations are assimilated to update only the ensemble mean by

$$\bar{\mathbf{x}}^a = \bar{\mathbf{x}}^f + \mathbf{K}[\mathbf{y}^o - H(\bar{\mathbf{x}}^f)] \quad (1)$$

where  $\bar{\mathbf{x}}^a$ ,  $\bar{\mathbf{x}}^f$  are the ensemble mean of analysis and background (forecast) respectively,  $\mathbf{K}$  the Kalman gain,  $\mathbf{y}^o$  the observations and  $H(\bullet)$  the observation operator. Here we use the superindex  $f$  rather than  $b$  to denote the background (forecasts) in order to avoid confusion with the subindex  $b$  used to denote the bias in the next section.

The ensemble perturbations are updated by transforming the background perturbations through a transform matrix  $\mathbf{T}$ , as proposed by Bishop et al. (2001)

$$\mathbf{X}^a = \mathbf{X}^f \mathbf{T} \quad (2)$$

where  $\mathbf{X}^a, \mathbf{X}^f$  are the analysis and background ensemble perturbations

(matrices whose columns are the difference between the ensemble members and the ensemble mean), and the error covariances are given by  $\mathbf{P}^{a,f} = \mathbf{X}^{a,f} (\mathbf{X}^{a,f})^T$ .

In the LETKF, the Kalman gain and transform matrix are given by

$$\mathbf{K} = \mathbf{X}^f \tilde{\mathbf{P}}^a (\mathbf{H}\mathbf{X}^f)^T \mathbf{R}^{-1} \quad (3)$$

$$\mathbf{T} = [(\mathbf{K} - \mathbf{I})\tilde{\mathbf{P}}^a]^{1/2} \quad (4)$$

where  $\tilde{\mathbf{P}}^a$ , the analysis error covariance in ensemble space, is given by

$$\tilde{\mathbf{P}}^a = [(\mathbf{K} - \mathbf{I})\mathbf{I} + (\mathbf{H}\mathbf{X}^f)^T \mathbf{R}^{-1} (\mathbf{H}\mathbf{X}^f)]^{-1} \quad (5)$$

with dimension  $K \times K$ , where the ensemble size  $K$  is usually much smaller than both the dimension of the model and the number of observations. As a result, the LETKF performs the analysis in the space spanned by the forecast ensemble members, which greatly reduces the computational cost. The LETKF is computed locally for each grid point by choosing the observations that will influence that grid point. More details about the LETKF are available in Hunt et al. (2007) and Szunyogh et al. (2008).

### 3. Methods to deal with model errors

#### 3.1. Multiplicative inflation

Multiplicative inflation simply inflates the ensemble error covariance  $\mathbf{P}_e^f$  by a factor  $1+\Delta$  to approximate the ‘true’ error covariance  $\mathbf{P}^f$

$$\mathbf{P}^f \leftarrow (1 + \Delta)\mathbf{P}_e^f \quad (6)$$

where  $\Delta$  is a tunable parameter. Equation (6) provides an increase in the ensemble covariance  $\mathbf{P}_e^f$  to account for the model errors that are not included in the original  $\mathbf{P}_e^f$ .

This method implicitly assumes that model errors have the same error structure as the internal errors so that their error covariance is proportional to the dynamically evolved error covariance  $\mathbf{P}_e^f$ .

### 3.2. Additive inflation

Additive inflation parameterizes model errors by adding random perturbations with a certain covariance structure to each ensemble member. Following Whitaker et al. (2008), in this study we randomly select samples from a subset of NCEP/NCAR (NNR hereafter, Kalnay et al. 1996) 6-hour tendency fields in January and February for the years 1982-1986. Unlike random numbers, these randomly selected tendency fields are geostrophically balanced. In each analysis cycle, we randomly select  $K$  tendency fields, remove their mean, scale these zero-mean fields, and add each of these scaled fields to one background ensemble member, i.e.,

$$\mathbf{x}_k^f = \mathbf{x}_{e(k)}^f + r\mathbf{q}_k \quad (7)$$

so that

$$\bar{\mathbf{q}}_k = 0 \quad (8)$$

and denote

$$\mathbf{q}_k \mathbf{q}_k^T = \mathbf{Q} \quad (9)$$

Here  $k$  is the index for each ensemble member, and  $\mathbf{x}_{e(k)}^f$  denotes the  $k$ th ensemble forecast.  $\mathbf{q}_k$  is the additive field added to ensemble member  $k$ , and  $r$  is its amplitude, a tunable parameter. Our procedure for making the additive fields is similar to that of Whitaker et al. (2008) ensuring that the added fields will only

enlarge the background error covariance by  $\mathbf{Q}$  and will not change the ensemble mean.

### 3.3. Dee and da Silva bias estimation method (DdSM)

Dee and da Silva (1998) developed a two-stage bias estimation algorithm, in which the estimation procedures for the bias and the state are carried out successively.

At the first step bias is estimated on every model grid point by

$$\mathbf{b}^a = \mathbf{b}^f - \mathbf{K}_b [\mathbf{y}^o - H(\mathbf{x}^f - \mathbf{b}^f)] \quad (10)$$

$$\mathbf{K}_b = \mathbf{P}_{bb}^f \mathbf{H}^T [\mathbf{H} \mathbf{P}_{bb}^f \mathbf{H}^T + \mathbf{H} \mathbf{P}_{xx}^f \mathbf{H}^T + \mathbf{R}]^{-1} \quad (11)$$

where the matrix  $\mathbf{P}_{xx}^f$  and  $\mathbf{P}_{bb}^f$  is the forecast error covariance for the state variables and for the bias respectively.

In practice the bias forecast error covariance  $\mathbf{P}_{bb}^f$  is unknown, so that following Dee and da Silva (1998) we assume that

$$\mathbf{P}_{bb}^f = \alpha \mathbf{P}_{xx}^f \quad (12)$$

Substituting (12) into (11), we have

$$\mathbf{K}_b = \alpha \mathbf{P}_{xx}^f \mathbf{H}^T [(1 + \alpha) \mathbf{H} \mathbf{P}_{xx}^f \mathbf{H}^T + \mathbf{R}]^{-1} \quad (13)$$

where  $\alpha$  is a tunable parameter.

In the second step, the analysis for the state variables is obtained using the standard analysis procedure with the unbiased forecast state  $\mathbf{x}^f - \mathbf{b}^a$

$$\mathbf{x}^a = (\mathbf{x}^f - \mathbf{b}^a) + \mathbf{K}_x [\mathbf{y}^o - H(\mathbf{x}^f - \mathbf{b}^a)] \quad (14)$$

$$\mathbf{K}_x = \mathbf{P}_{xx}^f \mathbf{H}^T (\mathbf{H} \mathbf{P}_{xx}^f \mathbf{H}^T + \mathbf{R})^{-1} \quad (15)$$

As for the bias forecast model, following Carton et al. (2000) we will use a

damped persistence,

$$\mathbf{b}_i^f = \mu \mathbf{b}_{i-1}^a \quad (16)$$

where  $i$  denotes time step, and  $\mu < 1$ , a tunable parameter

The cost of the DdSM is about twice that of no bias estimation, since the updated equations are solved twice, first for the bias estimation and then for the state variables. However, this double cost problem can be avoided if  $\alpha \ll 1$  in which case (13) becomes

$$\begin{aligned} \mathbf{K}_b &\approx \alpha \mathbf{P}_{xx}^f \mathbf{H}^T [\mathbf{H} \mathbf{P}_{xx}^f \mathbf{H}^T + \mathbf{R}]^{-1} \\ &= \alpha \mathbf{K}_x \end{aligned} \quad (17)$$

Reversing the order of the bias estimation step and that of the state analysis step, we obtain a simplified version of the DdSM (Radakovich et al. 2001).

$$\mathbf{x}^a = (\mathbf{x}^f - \mathbf{b}^f) + \mathbf{K}_x [\mathbf{y}^o - H(\mathbf{x}^f - \mathbf{b}^f)] \quad (18)$$

$$\mathbf{b}^a = \mathbf{b}^f - \alpha \mathbf{K}_x [\mathbf{y}^o - H(\mathbf{x}^f - \mathbf{b}^f)] \quad (19)$$

In this approach the computation of (19) is almost cost free after the state analysis  $\mathbf{x}^a$  has been updated by (18), since  $\mathbf{K}_x [\mathbf{y}^o - H(\mathbf{x}^f - \mathbf{b}^f)]$  is simply the analysis increment for the state variables.

Above we give the general equations for the DdSM and its simplified version. In the application of the DdSM to an EnKF system, no additional ensemble members are required for the bias since the bias forecast error covariance  $\mathbf{P}_{bb}^f$  is obtained directly from the state forecast error covariance  $\mathbf{P}_{xx}^f$ . Therefore, the term  $\mathbf{x}^f$  in equation (10) and (19) is actually the ensemble mean of forecasts.

### 3.4. Low-Dimensional Method (LDM)

We assume the NCEP/NCAR reanalysis (NNR) as a reference field to approximate the atmospheric truth, and conduct the reference forecast which is pure 6-hour model forecast starting from the NNR without doing any data assimilation. The (apparent) 6-hour forecast error  $\mathbf{x}^e$  is then defined as the difference between the reference forecast and the NNR valid at the same time.

The low-dimensional scheme (Danforth et al. 2007) assumes that model error  $\mathbf{x}_m^e$  has three components, namely the bias, periodic errors dominated by errors in the diurnal cycle, and model errors that are state-dependent:

$$\mathbf{x}_m^e(t) = \mathbf{b} + \sum_{l=1}^L \beta_l(t) \mathbf{e}_l + \sum_{n=1}^N \gamma_n(t) \mathbf{f}_n \quad (20)$$

in which  $t$  denotes the time step. The forecast bias  $\mathbf{b}$  is obtained by averaging the forecast errors  $\mathbf{x}^e$  over a certain training time period  $\mathbf{b} = \langle \mathbf{x}^e \rangle$ , and the leading EOFs  $\mathbf{e}_l$  from the anomalous error field  $\mathbf{x}^{e'} = \mathbf{x}^e - \langle \mathbf{x}^e \rangle$  are used to estimate diurnal or other periodic errors. The state-dependent model error component is given by the leading SVD modes (SVDs)  $\mathbf{f}_n$  of the covariance of the coupled model state anomalies  $\mathbf{x}^{f'} = \mathbf{x}^f - \langle \mathbf{x}^f \rangle$  and corresponding error anomalies  $\mathbf{x}^{e'}$ .  $L$  and  $N$  are the number of retained leading modes of EOFs and SVDs, respectively. The spatial fields  $\mathbf{b}$ ,  $\mathbf{e}_l$  and  $\mathbf{f}_n$  are time-independent and computed offline using the samples in the training period. We call this approach low-dimensional because the shape of the model errors is pre-estimated separately and only their amplitudes  $\beta_l(t)$  and  $\gamma_n(t)$  which have a much lower dimension ( $L$  and  $N$ ) than the full model dimension, are

estimated online.

During the training period, the time-series of  $\beta_l$  is calculated by projecting  $\mathbf{x}^{e_l}$  onto the EOFs  $\mathbf{e}_l$ . Since  $\beta_l$  is dominated by the bias in the diurnal cycle, the time-dependent  $\beta_l(t)$  can be estimated by averaging the  $\beta_l$  over the diurnal cycle in the training period. For example, we can use the samples in the training period to calculate the average of  $\beta_l$  for 0000UTC, 0600UTC, 1200UTC and 1800UTC separately and time-interpolate them in the current time-step. For the calculation of the state-dependent component  $\sum_{n=1}^N \gamma_n(t) \mathbf{f}_n$  using Singular Value Decomposition, the readers are referred to Danforth et al. (2007).

#### 4. The LETKF performance in perfect model experiments

An AGCM model, the SPEEDY model (Molteni 2003) is used in this study. The SPEEDY model solves the primitive equation for prognostic variables of zonal wind ( $u$ ), meridional wind ( $v$ ), temperature ( $T$ ), specific humidity ( $q$ ), and surface pressure ( $p_s$ ) at the triangular truncation T30, corresponding to 96\*48 grid points and 7 sigma levels. First, we assume a perfect model where a nature run is generated by integrating the SPEEDY model from 0000 UTC 1 January, 1987, until 1800 UTC 15 February, 1987. The observations are simulated by adding normally-distributed random noise to the nature run, and are available at each model grid point for  $p_s$  and every second model grid point for  $u, v, T, q$ , in both the zonal and meridional directions, i.e., 25% of the number of model grid points. The amplitudes of the observation errors are 1 m/s for  $u, v$  wind, 1 K for  $T$ ,  $10^{-4}$  kg/kg for  $q$  and 1 hPa

for  $p_s$ . For each forecast-analysis cycle, the SPEEDY model is used to generate the 6-hour forecast and the observations are assimilated by the LETKF with 30 ensemble members and a  $\Delta=0.05$  multiplicative inflation parameter to deal with sample errors in the covariance. Figure 1 shows the time-series of Root-Mean-Square (RMS) analysis error (defined as analysis minus true state), averaged over the whole globe, for zonal wind ( $u$ ), geopotential height ( $Z$ ), temperature ( $T$ ), specific humidity ( $q$ ) at 500hPa and surface pressure ( $p_s$ ). It is clear that after the initial spin-up period, the analysis RMSE for all the variables is much smaller than the observational error standard deviations.

To investigate why the LETKF performs well, the background ensemble spread is compared with the background error. Carrying out perfect model experiments, the true background error with respect to the nature run can be calculated. In order for the LETKF to perform well, the ensemble spread should be representative of the true background error. Figure 2 shows the 500hPa height background ensemble mean error field (shaded) and the ensemble spread (contour) at 1200 UTC 3 February, 1987, an arbitrarily chosen time. These two fields, although noisy, agree generally with each other in location. Then we compare the background RMSE of the height field and the corresponding spread averaged over the whole globe (Figure 3). The spread is slightly smaller at low levels and slightly larger in the upper levels compared to the background RMSE, but still they are quite close. Figure 2 and 3 together demonstrate that the spread among 30 ensemble members has captured the true background error well in both structure and magnitude.

## 5. Accounting for and correcting model errors in the LETKF

To assess the performance of the LETKF in the presence of model errors, we replace the nature run in the perfect model experiments by the NNR fields. Since the NNR assimilated real observations, we assume that the NNR fields are an approximate estimate of the unknown ‘true’ atmosphere. A quantitative validation of this assumption is beyond the scope of this research. Random noises with the same standard deviation used in the perfect model experiments are added to simulate ‘NNR observations’. The density of observations remains the same as that in the perfect model experiments.

### 5.1. Effects of model errors on the LETKF

Serving as a benchmark, the control run is carried out using the same configuration ( $\Delta=0.05$  and 30 ensemble members) as that in section 4 but replacing the observations generated from the nature run with the ‘NNR observations’. No additional method is applied to deal with model errors. After an initial spin-up period of 15 days, the analyses and forecasts are verified against the NNR.

The strong negative influence of the model errors on the performance of the LETKF is very clear in the control run (results not shown). In the presence of model errors and without accounting for them, the 500 hPa height analysis RMSE increases from 2.4 m (in the perfect model) to 50 m due to the model errors and their accumulated effects. An increase by more than an order of magnitude is also observed for other variables and regions. However, it should be noted that with a more

sophisticated and high-resolution numerical model, such as those currently used in operational centers, the negative impact of model errors would be much smaller.

The background ensemble spread of the height field is plotted in Figure 4 to investigate why the LETKF performs poorly in the presence of large model errors. It is interesting to find that the spread is very close to that obtained in the perfect model experiment, while ideally it should be as large as the actual forecast error, as it happens for a perfect model. This result indicates that when using the same model, the forecast ensembles are “blind” to model errors, and therefore the ensemble spread underestimates the actual forecast error, leading to excessive confidence in the forecasts, less weight given to the observations and, as a result, to the poor performance of the LETKF.

## 5.2. Accounting for and correcting model errors

Different methods described in section 3 are applied to the SPEEDY-LETKF system to account for model errors. As in the control run, experiments are implemented for the period 0000 UTC 1 January, 1987 to 1800 UTC 15 February, 1987 and the verification statistics are computed for analyses and forecasts against the NNR fields after the initial spin-up period of 15 days.

### 5.2.1. Multiplicative inflation versus additive inflation

Figure 5 shows the analysis RMSE of 200 hPa  $u$ , 500 hPa  $Z$ , 850 hPa  $q$  and 925 hPa  $T$  fields, from multiplicative inflation (with an optimal parameter of

$\Delta = 1.5$ ), additive inflation (with an optimal amplitude of  $r=1.5$ ) and the control run . Both inflation schemes result in much better analyses than the control run for all the fields. As found in previous studies, e.g., Hamill and Whitaker (2005), Whitaker et al. (2008), additive inflation outperforms multiplicative inflation.

### 5.2.2. Dee and da Silva method combined with additive inflation (DdSM+)

The DdSM aims to estimate and correct model bias, but does not account for state-dependent and random errors. Since the performance of the additive inflation is better than that of the multiplicative inflation, we combine the DdSM with additive inflation to account for random system noise. The additive noise is obtained in the same way as that in additive inflation scheme. We refer to the DdSM augmented with additive noise as DdSM+.

Recall that there are two variables ( $\mu$  and  $\alpha$ ) to be tuned in the pure DdSM. If additive inflation is used to model the system-noise, the amplitude ( $r$ ) of additive noise is another parameter that also needs to be tuned. To simplify the task of tuning these three parameters, first we fix  $\alpha=0.5$  (following the recommendation of Dee and da Silva 1998) and  $\mu=1.0$  (assuming a persistence model for bias prediction) and then tune the amplitude ( $r$ ) of the additive noises. We start at 0000 UTC 1 January, 1987 by assuming zero bias and run the SPEEDY-LETKF system for 45 days. However, no matter how small  $r$  is, the filter diverges, especially for temperature fields in the lower levels, and the bigger  $r$ , the faster the divergence. Using the same SPEEDY-LETKF system but with pure DdSM ( $r=0$ ), Miyoshi (2005) observed

similar filter divergence for all choice of  $\alpha$  when fixing  $\mu=1.0$ . Thus, we let  $\mu$  be less than 1 to reduce the impact of bias from the previous time step and find  $\mu=0.9$  is successful for a wide range of choices for  $r$  and gives better results than  $\mu=0.8$ . Fixing  $\mu=0.9$ , the pairs of  $(\alpha, r)$  are tuned. The results are summarized in Table 1. It is clear that accounting for random system noise is essential in order for the LETKF to perform well. Without additive noise, the pure DdSM ( $r=0$ ) is not competitive with pure additive inflation ( $\alpha=0$ ) with an optimal amplitude of  $r=1.5$ . Using a small additive noise ( $r=0.25$ ), the DdSM+ outperforms the pure additive inflation scheme, but the optimal choice of  $\alpha$  is large ( $\alpha=0.75$ ). When  $r$  is increased to 0.5, the value of the optimal  $\alpha$  reduces to 0.5. These results can be better understood by the expression of  $\mathbf{P}_{bb}^f = \alpha \mathbf{P}_{xx}^f$  where  $\alpha$  is an explicit parameter and  $r$  is an implicit factor (through affecting  $\mathbf{P}_{xx}^f$ ) to determine the bias forecast error covariance  $\mathbf{P}_{bb}^f$ . When  $r$  is small, the system requires a big value of  $\alpha$  to obtain an optimal  $\mathbf{P}_{bb}^f$ , while as  $r$  increases, the optimal value of  $\alpha$  decreases because the forecast error covariance  $\mathbf{P}_{xx}^f$  for the state variables has already been increased. By increasing  $r$  from zero to 0.5, a large improvement is found. Beyond  $r=0.5$ , there is little further improvement. As shown in Table 1, we choose  $(\mu = 0.9, \alpha = 0.5, r = 0.6)$  as the optimal setting of the parameters for the DdSM+ .

We take the same setting of the parameters ( $\mu = 0.9, \alpha = 0.5, r = 0.6$ ) and run the SPEEDY-LETKF system with the simplified DdSM+ (the simplified DdSM, Radakovich et al. 2001, augmented by additive noise). Although the choice  $\alpha=0.5$  does not satisfy the condition  $\alpha \ll 1$  stated in section 3 for the simplified DdSM,

tuning  $r$  using a smaller value  $\alpha=0.1$ , actually gives much worse results than with  $\alpha=0.5$ . This is possibly due to a suboptimal analysis increment when forcing  $\alpha$  to be a small value in equation (19). Therefore, we keep the setting of ( $\mu = 0.9$ ,  $\alpha=0.5$ ,  $r=0.6$ ) here. The resulting analysis is worse than that from the DdSM+ for all the variables but better than that from pure additive inflation in the 500 hPa height field. Comparable results are found in the other fields, except for specific humidity (Table 2).

### 5.2.3. LDM with additive inflation (LDM+)

Since experiments are carried out for January and February in 1987, the 5-year climatology of the same months for the years 1982-1986 is chosen as the training period, following Danforth et al. (2007). In this training period, the 6-hour SPEEDY forecasts initialized with the NNR fields are conducted and then the samples of forecast error  $\mathbf{x}^e$  are obtained by taking the differences between the SPEEDY 6-hour forecasts and the NNR fields valid at the same time.

Three types of model errors in equation (20) with LDM are corrected but, as it was the case with the pure DdSM, the pure LDM without accounting for system noise is not able to beat pure additive inflation (Figure 6). To parameterize system-noise, randomly selected NNR 6-hour tendency fields are added to each background ensemble member and their amplitude are tuned as what has been done in the DdSM+ scheme. As seen in Figure 6, the LDM, plus a small amount ( $r=0.4$ ) of additive noise (LDM+ hereafter) significantly outperforms the pure additive inflation scheme, suggesting the necessity to deal with both model bias and system-noise in the

presence of complicated model errors.

#### 5.2.4. Overall comparison

Finally all the methods with their optimal configurations are compared with each other. As before, the results are verified against the NNR fields.

##### *a. Analysis verification*

Figure 7 illustrates that the LDM+ provides significantly better analyses than the other methods for all the variables and at all levels. The DdSM+ generally outperforms both inflation schemes. Its simplified version is worse than the original version but is comparable to the pure additive inflation (except for specific humidity) and better than the pure multiplicative inflation scheme, which produces the worst results of all five methods. However, it should be noted that all the methods have made major analysis improvements compared to the control run (gray dotted curve in Figure 8). Correcting model biases is, in general, better than only accounting for their effects in the second moment of the ensemble, assuming we have a good method to estimate model biases. Though the estimated biases are not good enough for the simplified DdSM+ to outperform the pure additive inflation scheme, the DdSM+ generally beats pure additive inflation. Among all methods, the LDM+ is the best: it outperforms other methods in all the fields throughout all pressure levels, especially at lower levels.

##### *b. 48-hour forecast verification*

So far we have focused on the comparisons in terms of the analysis accuracy. However, the goal of developing more accurate analyses is to improve the short-term

forecasts. Within an imperfect model, the short-term forecast errors come from both growing errors in the initial condition and model deficiencies. Although the model errors could be corrected within the forecast model, here we would like to see if the advantage of one method in the data assimilation process can be retained over a forecast period. Otherwise, there would be no benefit in improving the initial analysis on short-term forecasts. Figure 9 shows the global-averaged 48-hour forecast RMSE at all pressure levels. The advantage of DdSM+ over additive inflation becomes less obvious for most fields, but remains significant for geopotential height fields at all levels. The large advantage of the LDM+ over the other two methods also decreases due to the contamination of the model errors. Nevertheless, it is still quite obvious and significant, except for the zonal wind above 200 hPa and the humidity above 700hPa.

Above we focused on the impact of initial analysis on the short-term forecast and did not attempt to correct the model errors during the forecast process. The LDM can also be used to estimate and correct the short-term model errors in the forecast phase, as shown by Danforth et al. (2007) with the SPEEDY model.

### 5.3. Sensitivity to observational network

Thus far, methods have been compared using a globally uniform observation network (the upper right panel in Figure 10), as if they were based only on satellite observations, resulting in uniform error fields (not shown). However, in reality there are more rawinsonde observations over land and fewer over the ocean. To investigate the sensitivity of each method to the choice of observational system, we apply a

rawinsonde-like network (the upper left panel in Figure 10) for  $u, v, T, q$  ( $p_s$  is still available everywhere) to pure additive inflation, the DdSM+ and the LDM+. We re-tune the parameters and choose the optimal setting for each method. Figure 10 (lower left panel) shows the zonal and time-averaged latitudinal profiles of geopotential height analysis RMSE at 500 hPa for the three methods with rawinsonde-like observation network. For comparison, the results from experiments described in subsection 5.2 with a uniform observation network are shown in the lower right panel. Using uniform observations, the performance of each method is less latitude-dependent. With rawinsonde-like observations, though the DdSM+ is still better than pure additive inflation, both are far more sensitive to observation density than LDM+. In the Southern Hemisphere and the northern polar region where few observations are available, the DdSM+ and pure additive inflation behave much worse than that of LDM+. Figure 10 demonstrate that the DdSM+ and pure additive inflation schemes are more sensitive to the choice of observation network, and perform poorly in regions with sparse observations, while the LDM+ is more robust. These results are not unexpected since the LDM+ bias correction is done in model space while the DdSM+ is performed in observation space. Large additive inflation is not helpful in regions where there are no observations.

## 6. Summary and Discussion

In this study we addressed the issue of model errors with the ensemble Kalman filter. Though focusing on the LETKF, an efficient approach within the EnKF family,

the results are applicable to other EnKF systems. First, we performed data assimilation experiments using the LETKF with the SPEEDY model under a perfect model scenario. It is found that the LETKF works very well in this ideal case. Then we dropped the perfect model assumption by assimilating observations generated from the NCEP/NCAR reanalysis fields. Without any additional effort to handle model errors, the performance of the LETKF is seriously degraded. The background ensemble spread is similar to that in the perfect model and therefore much smaller than the true forecast error (that now includes model errors). The “blindness” of the LETKF to model error is likely due to the fact that each ensemble member is integrated with the same model. If forecasts from different systems are available, as in the super-ensemble of Krishnamurti et al. (2000), we would expect to be able to at least partially represent model errors.

We investigated two simple ways to represent the effect of model errors and two sophisticated methods to estimate and remove model bias. Our results suggest that multiplicative inflation is worse than additive inflation. The pure bias removal methods (DdSM and LDM) remove model bias, but cannot handle system noise; as a result, they are not able to beat inflation schemes that account for the total model errors. Supplemented by additive noise in order to be able to represent the system noise, bias removal methods generally outperform the pure inflation schemes. Of all these methods, the low-dimensional method with additive inflation (LDM+) where the time-averaged model bias, diurnal bias and state-dependent errors are estimated from a large number of 6-hour forecast errors, gives the most accurate analyses and

48-hour forecasts. The advantage of the LDM+ over other methods is larger in data sparse regions than in data dense regions due to the fact that its bias correction is done in model space and thus less sensitive to the absence of abundant observations. We note that in training the LDM we have used a long reanalysis that has spread information from both satellite and rawinsonde observations throughout the atmosphere.

Although the DdSM combined with inflation (DdSM+) produces worse results than the LDM+, it is generally superior to both pure inflation schemes. The disadvantages of DdSM+ are the doubling of the computational cost and exclusive reliance on observations. When the observations are sparse, the impact of the bias correction is limited. In the worst case, where the observations themselves are biased, it is not at all obvious that this algorithm can work correctly. Our results of LDM estimation may be too optimistic, since in our applications we assume the NNR field is an approximation of the unknown truth and use it to generate the samples of model errors during the training period. In reality, the NNR field could be biased and generating good samples of model errors is a challenge to the LDM+. It is not clear in the real world whether the model error samples generated from the NNR fields are good enough to represent the true model errors. In practice, we could use a more advanced reanalysis, like ERA-40 or JRA-25 to replace the NNR. We could also verify the analysis against a more advanced reanalysis, and thus simulate the fact that the truth is not available for the training. The EnKF analysis increments could also be used as model error samples. For the training of error samples, iterations are required

since at first the analyses are also biased, so that the analysis increments cannot sample model error well. We intend to explore this idea with the SPEEDY model to see whether the final model error samples after convergence are good enough to represent the true model errors.

**Acknowledgements:** The authors are very grateful to the members of the Chaos-Weather group at the University of Maryland for helpful discussions, and to two anonymous reviewers for their constructive suggestions that helped us improve the manuscript. This research was partially supported by 973 Program (2009CB421500), NASA grant NNG04G29G, NOAA grant NA04OAR4310103 and CMA grant GYHY200806029.

## References

- Anderson, J. L., and S. L. Anderson, 1999: A Monte Carlo implementation of the non-linear filtering problem to produce ensemble assimilations and forecasts. *Mon. Wea. Rev.*, **127**, 2741–2758.
- Baek, S.-J., B. R., Hunt, E. Kalnay, E. Ott, and I. Szunyogh, 2006: Local ensemble Kalman filtering in the presence of model bias, *Tellus A*, **58**, 293-306.
- Bishop, C. H., B. J. Etherton, and S. J. Majumdar, 2001: Adaptive sampling with the ensemble transform Kalman filter. Part I: Theoretical aspects. *Mon. Wea. Rev.*, **129**, 420-436.
- Carton, J. A, G. Chepurin, X. Cao and B. Giese, 2000: A simple ocean data assimilation analysis of the global upper ocean 1950-95. Part I: Methodology. *J. Phys. Oceanogr.*, **30**, 294-309.
- Chepurin, G. A., J. A. Carton, and D. Dee, 2005: Forecast model bias correction in ocean data assimilation. *Mon. Wea. Rev.*, **133**, 1328–1342.
- Corazza, M., E. Kalnay, and S.-C. Yang, 2007: An implementation of the local ensemble Kalman filter in a quasi geostrophic model and comparison with 3D-Var. *Nonlinear Processes in Geophysics*, **14**, 89-101.
- Danforth, C. M., and E. Kalnay, 2008: Using singular value decomposition to parameterize state-dependent model errors. *J. Atmos. Sci.*, **65**, 1467-1478.
- , ———, and T. Miyoshi, 2007: Estimating and correcting global weather model error. *Mon. Wea. Rev.*, **135**, 281-299.
- Dee, D. P., 1995: On-line estimation of error covariance parameters for atmospheric

- data assimilation. *Mon. Wea. Rev.*, **123**, 1128-1145.
- , and A. M. da Silva, 1998: Data assimilation in the presence of forecast bias. *Quart. J. Roy. Meteor. Soc.*, **124**, 269-295.
- , and R. Todling, 2000: Data assimilation in the presence of forecast bias: the GEOS moisture analysis. *Mon. Wea. Rev.*, **128**, 3268–3282.
- Evensen, G., 1994: Sequential data assimilation with a nonlinear quasi-geostrophic model using Monte Carlo methods to forecast error statistics. *J. Geophys. Res.*, **99** (C5), 10143-10162.
- Hamill, T. M., and J. S. Whitaker, 2005: Accounting for the error due to unresolved scales in ensemble data assimilation: A comparison of different approaches. *Mon. Wea. Rev.*, **133**, 3132-3147.
- Houtekamer, P. L., and H. L. Mitchell, 2005: Ensemble Kalman filtering. *Quart. J. Roy. Meteor. Soc.*, **131**, 3269-3289.
- , ——, G. Pellerin, M. Buehner, M. Charron, L. Spacek, and B. Hansen, 2005: Atmospheric data assimilation with an ensemble Kalman filter: Results with real observations. *Mon. Wea. Rev.*, **133**, 604-620.
- Hunt, B. R., E. Kostelich, I. Szunyogh, 2007: Efficient data assimilation for spatiotemporal chaos: a local ensemble transform Kalman filter. *Physica D*, **230**, 112-126.
- Fujita, T., D. J. Stensrud, and D.C. Dowell, 2007: Surface data assimilation using an ensemble Kalman filter approach with initial condition and model physics uncertainties. *Mon. Wea. Rev.*, **135**, 1846-1868.

- Kalnay, E., and Coauthors, 1996: The NMC/NCAR 40-Year Reanalysis Project. *Bull. Amer. Meteor. Soc.*, **77**, 437–471.
- Keppenne, C. L., M. M. Rienecker, N. P. Kurkowski, and D. A. Adamec, 2005: Ensemble Kalman filter assimilation of temperature and altimeter data with bias correction and application to seasonal prediction. *Nonlinear Processes in Geophysics*, **12**, 491–503.
- Krishnamurti, T. N., C. M. Kishtawal, Z. Zhang, T. LaRow, D. Bachiochi, E. Williford, S. Gadgil, and S. Surendran, 2000: Multimodel ensemble forecasts for weather and seasonal climate. *J. Climate*, **13**, 4196–4216.
- Meng, Z., and F. Zhang, 2007: Tests of an ensemble Kalman filter for mesoscale and regional-scale data assimilation. Part II: Imperfect model experiments. *Mon. Wea. Rev.*, **135**, 1403–1423.
- , and ———, 2008: Tests of an ensemble Kalman filter for mesoscale and regional-scale data assimilation. Part III: Comparison with 3DVAR in a real-data case study. *Mon. Wea. Rev.*, **136**, 522–540.
- Mitchell, H. L., and P. L. Houtekamer, 2000: An adaptive ensemble Kalman filter. *Mon. Wea. Rev.*, **128**, 416–433.
- , ———, and G. Pellerin, 2002: Ensemble size, balance, and model-error representation in an ensemble Kalman filter. *Mon. Wea. Rev.*, **130**, 2791–2808.
- Miyoshi, T. 2005: Ensemble Kalman filter experiments with a primitive-equation global model, PhD Thesis at the University of Maryland.

- Molteni, F., 2003: Atmospheric simulations using a GCM with simplified physical parametrizations. I: Model climatology and variability in multi-decadal experiments. *Climate Dyn.*, **20**, 175-191.
- Radakovich, J. D., P. R. Houser, A. M. da Silva, and M. G. Bosilovich, 2001: Results from global land-surface data assimilation methods. *Proceeding of the fifth symposium on integrated observing systems*, Albuquerque, NM, Amer. Meteor. Soc., 132-134.
- Szunyogh, I., E. J. Kostelich, G. Gyarmati, E. Kalnay, B. R. Hunt, E. Ott, E. Satterfield and J. A. Yorke, 2008: A local ensemble transform Kalman filter data assimilation system for the NCEP global model. *Tellus A*, **60**, 113-130.
- Tippett, M. K., J. L. Anderson, C. H. Bishop, T. M. Hamill, and J. S. Whitaker, 2003: Ensemble square root filters. *Mon. Wea. Rev.*, **131**, 1485-1490.
- Torn R. D., and G. J. Hakim, 2008: Performance characteristics of a pseudo-operational ensemble Kalman filter. *Mon. Wea. Rev.*, **136**, 3947-3963.
- Whitaker, J. S., T. M. Hamill, X. Wei, Yucheng Song and Z. Toth, 2008: Ensemble data assimilation with the NCEP global forecasting system. *Mon. Wea. Rev.*, **136**, 463-482.

## Figure Captions

Figure 1. Time series of global-averaged analysis RMSE (solid curve) at 500 hPa for the period between 0000 UTC 1 January 1987 and 1800 UTC 15 February 1987 in a perfect model experiment. The observational error standard deviations are shown as dash lines wherever applicable. The five panels from the top to the bottom correspond to zonal wind, geopotential height, temperature, specific humidity and surface pressure, respectively.

Figure 2. The background (6-hour forecast) error field (in meters, shaded) and the ensemble spread of 500 hPa height field (in meters, contour) at 1200 UTC 3 February, 1987, an arbitrarily chosen time, in a perfect model experiment.

Figure 3. Background RMSE at all pressure levels (solid) and background ensemble spread (dashed) of height field, temporally averaged for one-month after the initial 15-day spin-up period in a perfect model experiment.

Figure 4. Background ensemble spread in height field at all pressure levels temporally averaged over a month after the initial 15-day spin-up period in the cases of perfect model, assimilating observations generated from the SPEEDY nature run (dashed), and imperfect model assimilating observations generated from the NNR field (solid).

Figure 5. Time series of the global-averaged analysis RMSE in the cases of the control run (dashed curve),  $\Delta=1.5$  multiplicative inflation (dotted curve) and  $r=1.5$

additive inflation (solid curve) assimilating the NNR observations. The four panels from the top to the bottom correspond to 200 hPa  $u$ , 500 hPa  $Z$ , 850 hPa  $q$  and 925 hPa  $T$  fields, respectively.

Figure 6. Time series of the global-averaged analysis RMSE of the 500 hPa  $Z$  and 925 hPa  $T$  fields, in the cases of the LDM alone (dashed curve),  $r=1.5$  additive inflation (dotted curve) and the LDM together with additive inflation with an amplitude  $r=0.4$  (solid curve).

Figure 7. Global-averaged analysis RMSE at all pressure levels in the cases of the LDM+ (black dotted), the DdSM+ (black dashed), additive inflation (black solid), the simplified DdSM+ (gray dashed) and multiplicative inflation (gray solid). The four panels correspond to u-wind field, temperature field, height field and specific humidity field, respectively. The averages are taken for a month after the initial half-month spin-up period.

Figure 8. Same as the top-left panel in Figure 7, but also shows the result for the control run (gray dotted) and for the perfect model experiment (black dot-dashed). We note that in a more realistic operational model, the negative effect of model errors would not as large as in this control run and a significant amount of inflation leads to better results even in the absence of bias correction (e.g., Szunyogh et al. 2008).

Figure 9. 48-hour forecast RMSE at all pressure levels in the cases of the LDM+ (dotted), the DdSM+ (dashed), and additive inflation (solid). The four panels correspond to u-wind field, temperature field, height field and specific humidity field, respectively. The averages are taken over all forecasts started every 6 hours between 0000 UTC 1 February 1987 and 1800 UTC 15 February 1987.

Figure 10. Upper panels: Observation locations in rawinsonde-like (left) and uniform (right) observation network. Lower panels: Zonal and time-averaged latitudinal profiles of geopotential height analysis RMSE at 500 hPa for additive inflation (dotted), the DdSM+ (solid) and the LDM+ (dashed), in the case of rawinsonde-like (left) and uniform (right) observation networks.

Table 1. Analysis RMSE of 500 hPa height (m) using the DdSM+ with different choices of  $(\alpha, r)$  with a fixed  $\mu=0.9$ . When  $r=0$  ( i.e., pure DdSM), a small parameter ( $\Delta=0.05$ ) of multiplicative inflation is applied in order to prevent filter divergence. For the other choices of  $r$ , no multiplicative inflation is used. For comparison, the pure addition inflation application is also shown ( $\alpha=0$  and  $r=1.5$ ).

$\alpha$	0.0	0.25	0.50	0.75	1.00
$r=0$			37.1	35.0	33.9
$r=0.25$		22.5	22.0	18.9	19.2
$r=0.5$		19.8	17.6	20.4	20.1
$r=0.6$			17.3		
$r=1.5$	23.8				

Table 2. Comparison of analysis RMSE between the applications of additive inflation, the DdSM+ and the simplified DdSM+. Results are shown for 200 hPa zonal wind ( $u$ ), 500 hPa height ( $Z$ ), 850 hPa specific humidity ( $q$ ) and 925 hPa temperature ( $T$ ) fields, temporally averaged for a month after the initial spin-up period.

Fields (unit)	200 hPa $u$ (m/s)	500 hPa $Z$ (m)	850 hPa $q$ (g/kg)	925 hPa $T$ (K)
Additive inflation	1.88	23.82	0.48	1.43
Simplified DdSM+	1.87	19.54	0.61	1.37
DdSM+	1.76	17.32	0.47	1.30

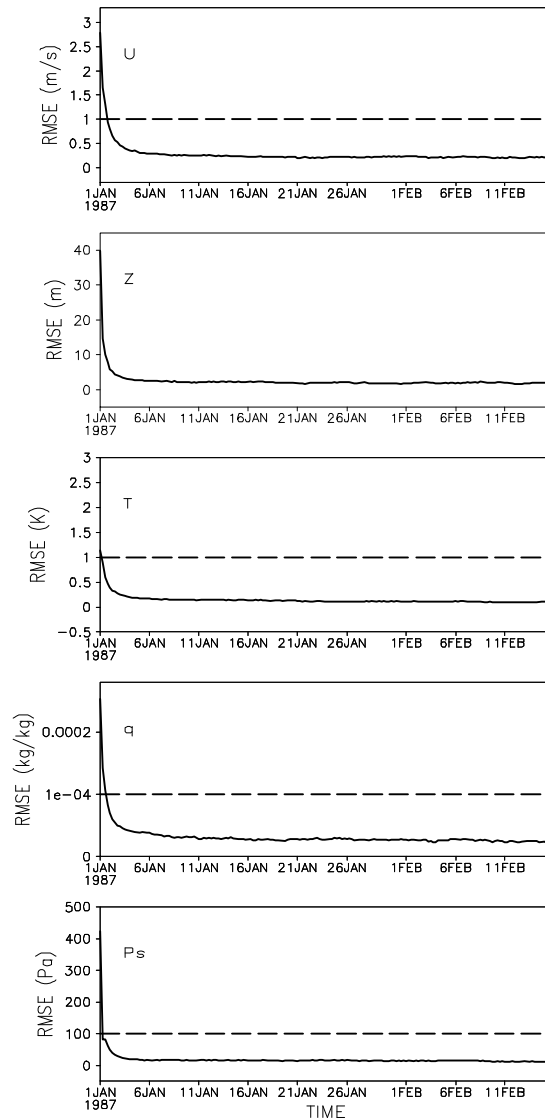


Figure 1. Time series of global-averaged analysis RMSE (solid curve) at 500 hPa for the period between 0000 UTC 1 January 1987 and 1800 UTC 15 February 1987 in a perfect model experiment. The observational error standard deviations are shown as dash lines wherever applicable. The five panels from the top to the bottom correspond to zonal wind, geopotential height, temperature, specific humidity and surface pressure, respectively.

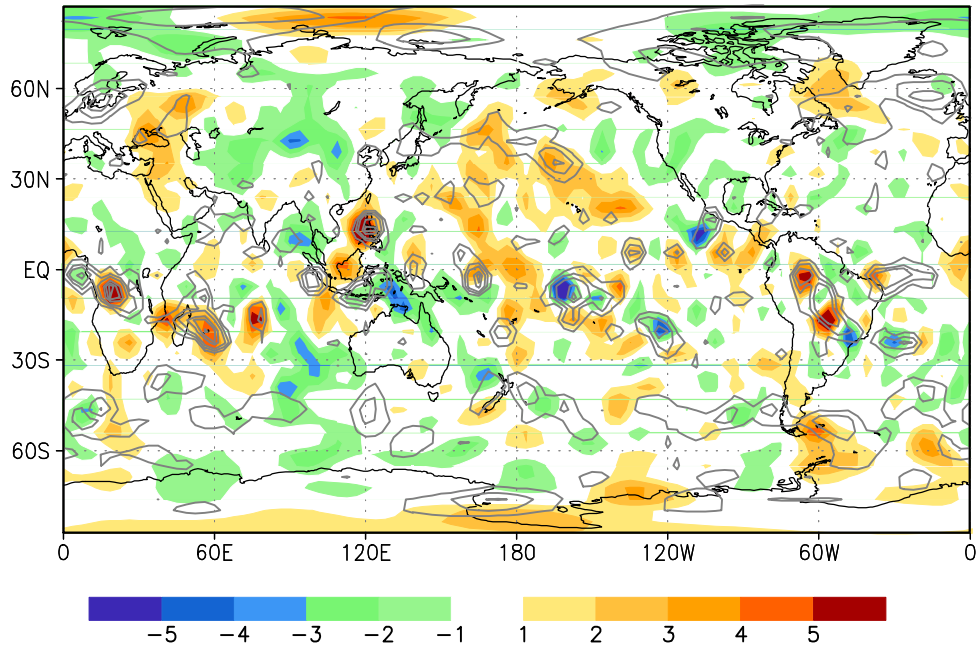


Figure 2. The background (6-hour forecast) error field (in meters, shaded) and the ensemble spread of 500 hPa height field (in meters, contour) at 1200 UTC 3 February, 1987, an arbitrarily chosen time, in a perfect model experiment.

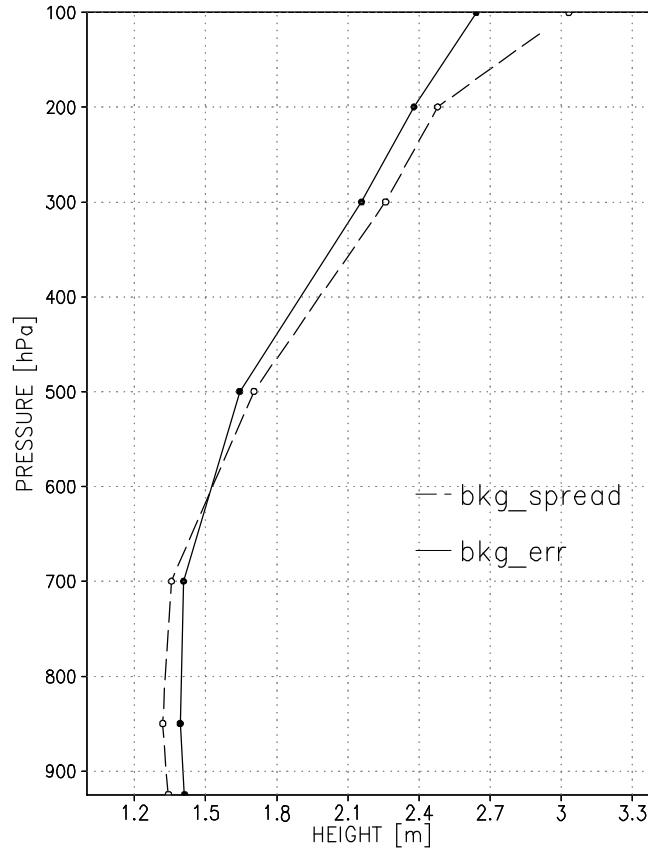


Figure 3. Background RMSE at all pressure levels (solid) and background ensemble spread (dashed) of height field, temporally averaged for one-month after the initial 15-day spin-up period in a perfect model experiment.

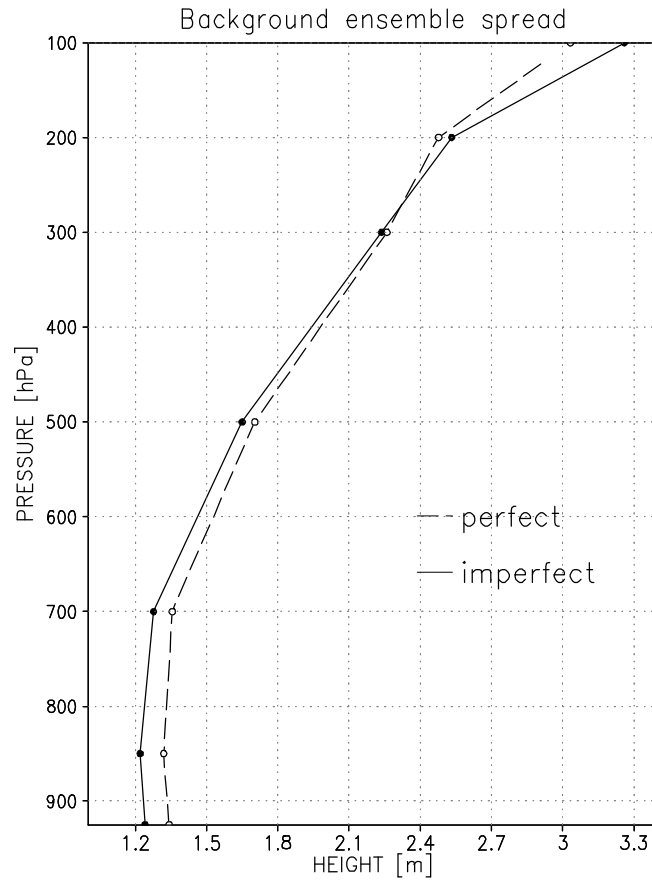


Figure 4. Background ensemble spread in height field at all pressure levels temporally averaged over a month after the initial 15-day spin-up period in the cases of perfect model, assimilating observations generated from the SPEEDY nature run (dashed), and imperfect model assimilating observations generated from the NNR field (solid).

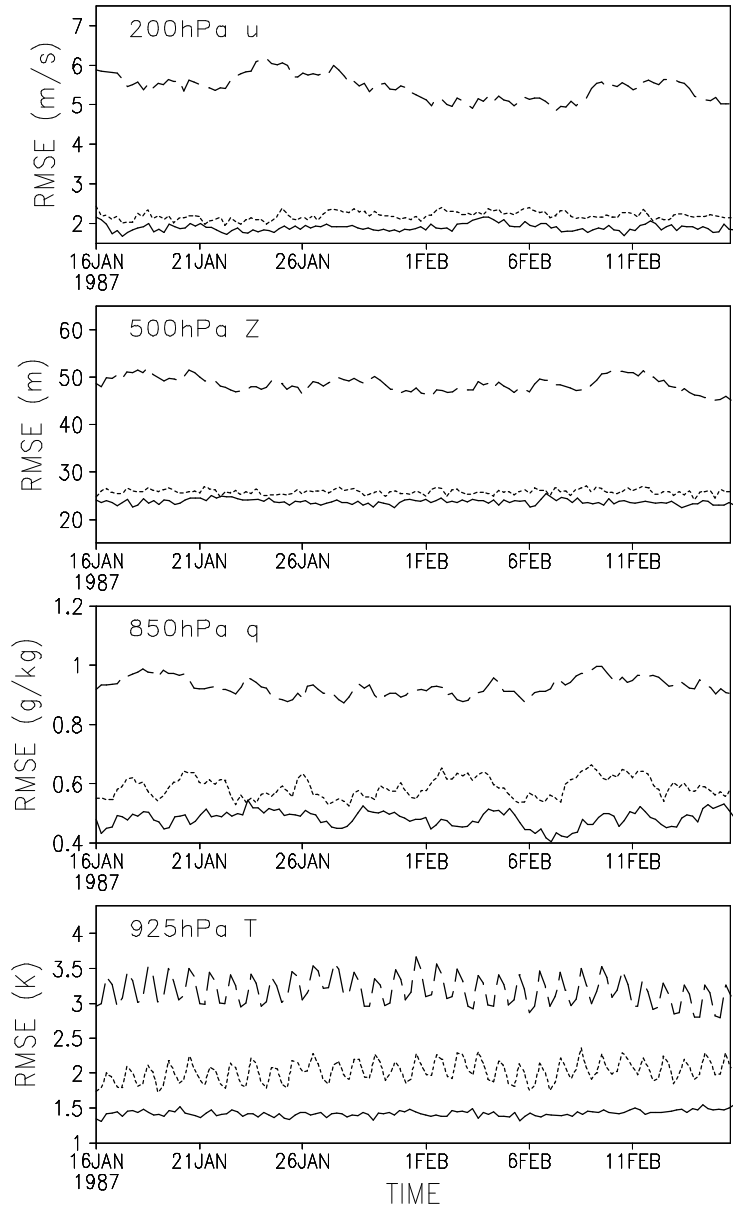


Figure 5. Time series of the global-averaged analysis RMSE in the cases of the control run (dashed curve),  $\Delta=1.5$  multiplicative inflation (dotted curve) and  $r=1.5$  additive inflation (solid curve) assimilating the NNR observations. The four panels from the top to the bottom correspond to 200 hPa  $u$ , 500 hPa  $Z$ , 850 hPa  $q$  and 925 hPa  $T$  fields, respectively.

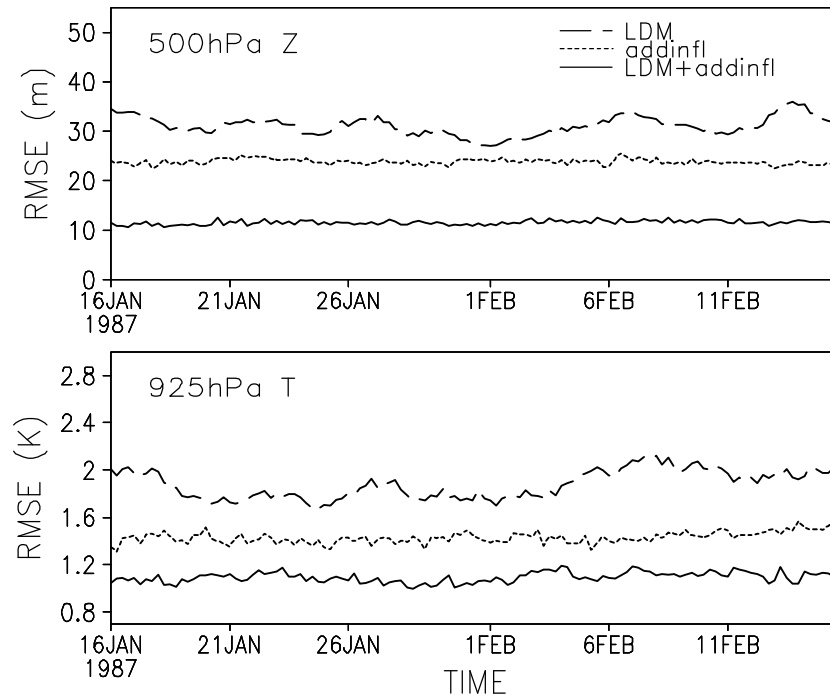


Figure 6. Time series of the global-averaged analysis RMSE of the 500 hPa  $Z$  and 925 hPa  $T$  fields, in the cases of the LDM alone (dashed curve),  $r=1.5$  additive inflation (dotted curve) and the LDM together with additive inflation with an amplitude  $r=0.4$  (solid curve).

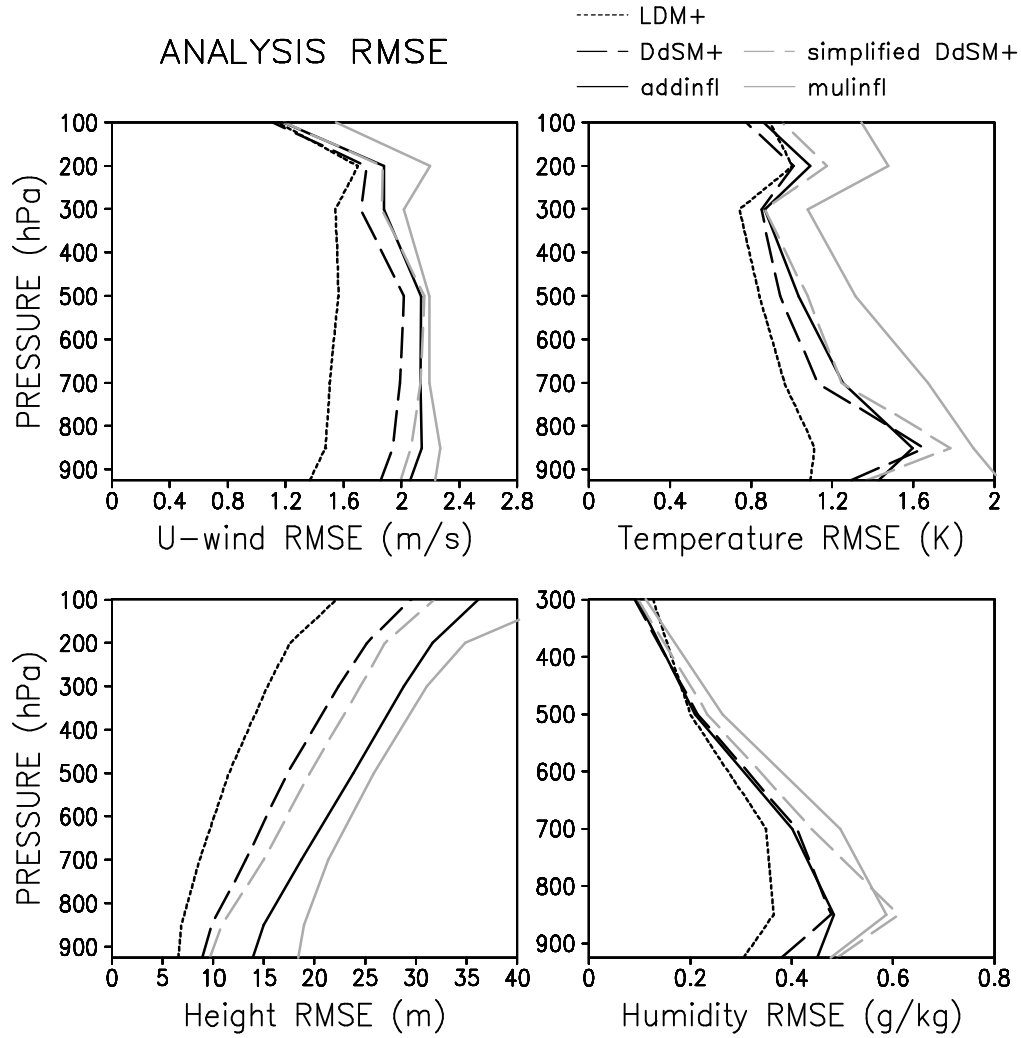


Figure 7. Global-averaged analysis RMSE at all pressure levels in the cases of the LDM+ (black dotted), the DdSM+ (black dashed), additive inflation (black solid), the simplified DdSM+ (gray dashed) and multiplicative inflation (gray solid). The four panels correspond to u-wind field, temperature field, height field and specific humidity field, respectively. The averages are taken for a month after the initial half-month spin-up period.

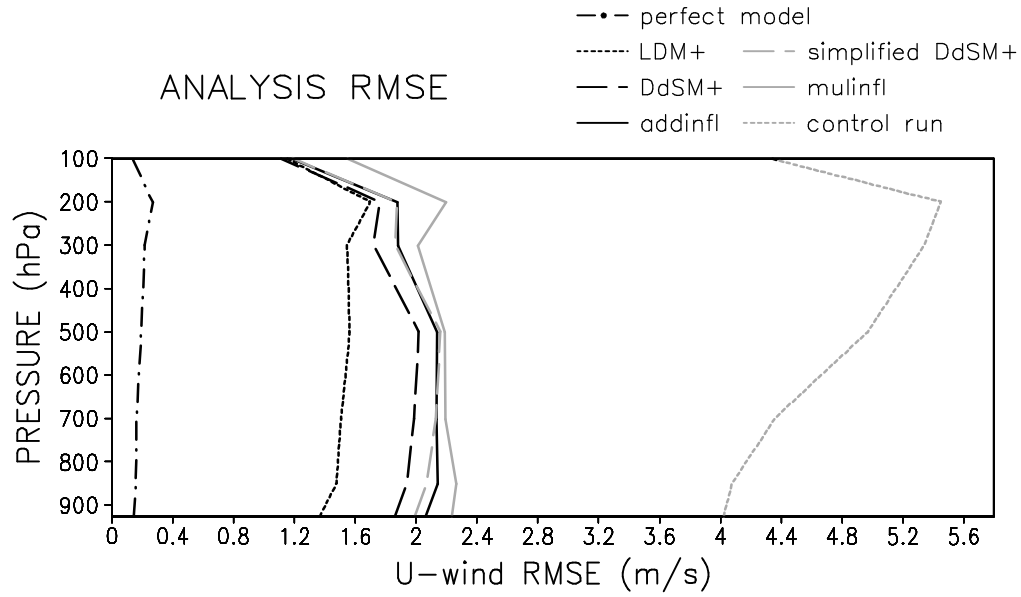


Figure 8. Same as the top-left panel in Figure 7, but also shows the result for the control run (gray dotted) and for the perfect model experiment (black dot-dashed). We note that in a more realistic operational model, the negative effect of model errors would not as large as in this control run and a significant amount of inflation leads to better results even in the absence of bias correction (e.g., Szunyogh et al. 2008).

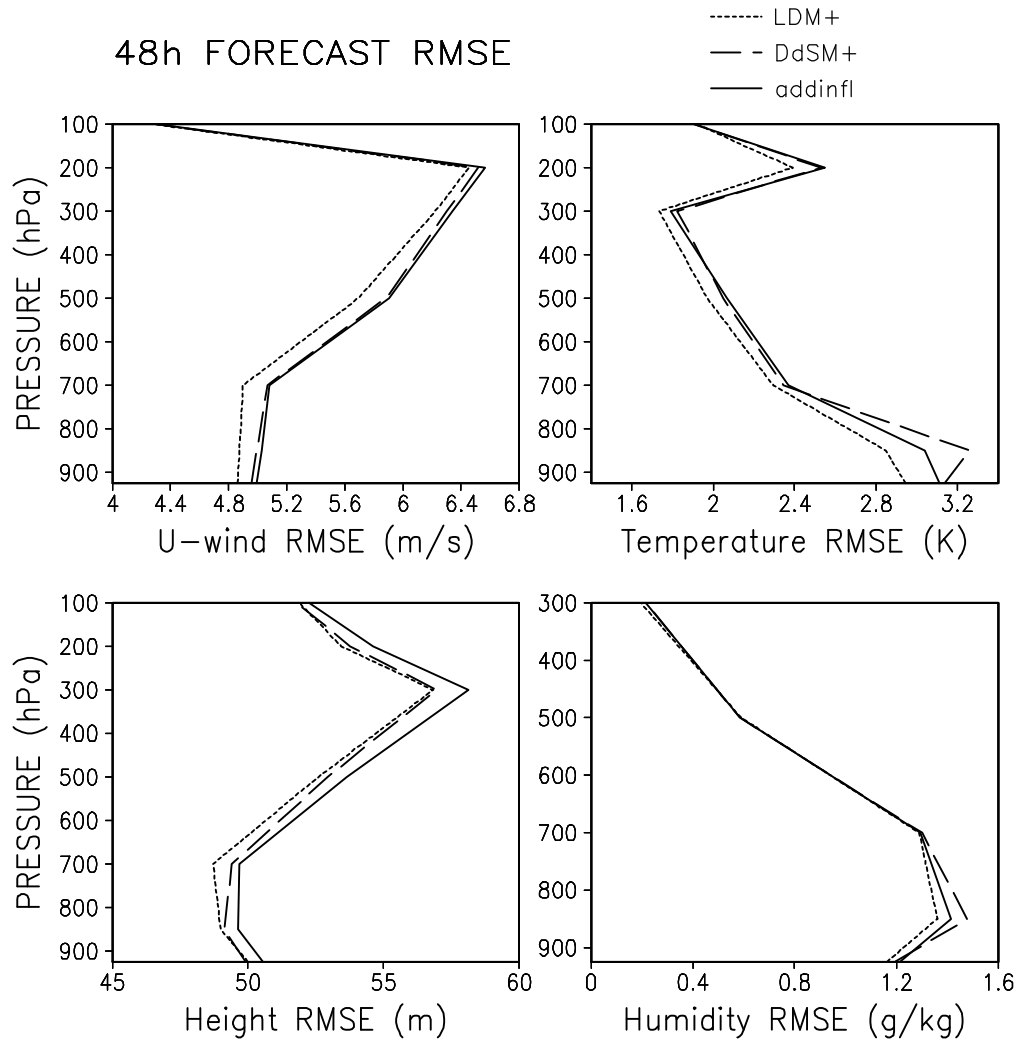


Figure 9. 48-hour forecast RMSE at all pressure levels in the cases of the LDM+ (dotted), the DdSM+ (dashed), and additive inflation (solid). The four panels correspond to u-wind field, temperature field, height field and specific humidity field, respectively. The averages are taken over all forecasts started every 6 hours between 0000 UTC 1 February 1987 and 1800 UTC 15 February 1987.

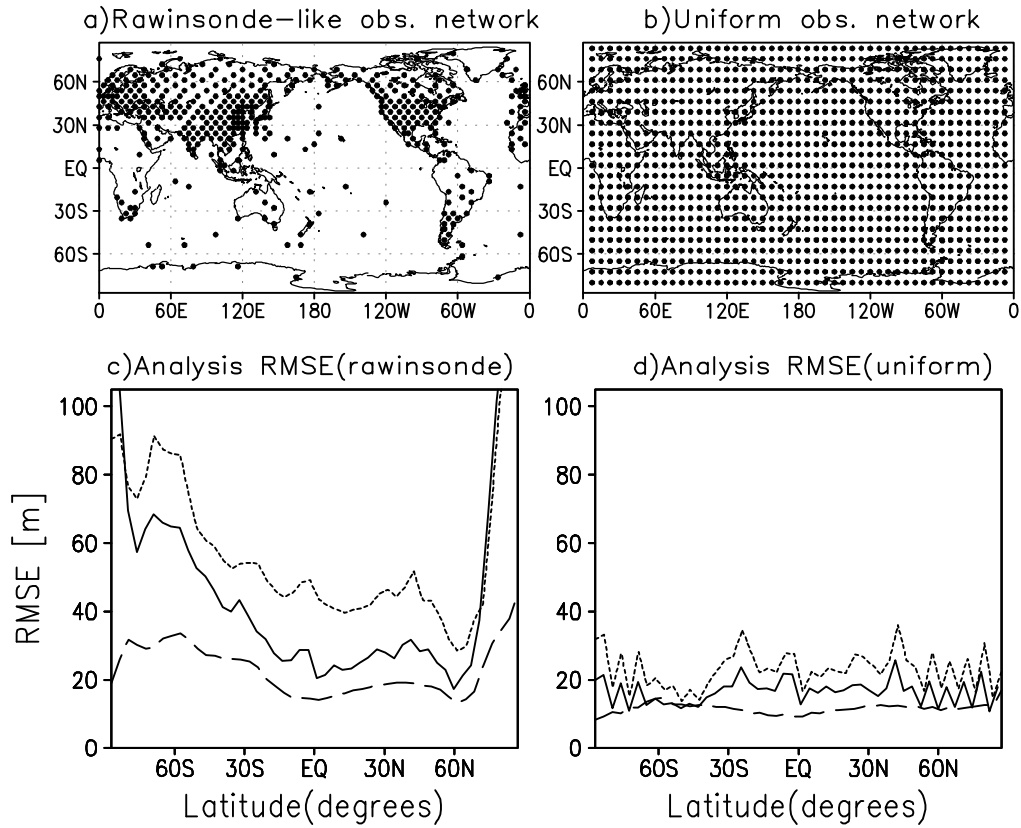


Figure 10. Upper panels: Observation locations in rawinsonde-like (left) and uniform (right) observation network. Lower panels: Zonal and time-averaged latitudinal profiles of geopotential height analysis RMSE at 500 hPa for additive inflation (dotted), the DdSM+ (solid) and the LDM+ (dashed), in the case of rawinsonde-like (left) and uniform (right) observation networks.